ACS APPLIED MATERIALS & INTERFACES

Research Article

www.acsami.org

Mapping the Anode Surface-Electrolyte Interphase: Investigating a Life Limiting Process of Lithium Primary Batteries

David C. Bock,[†] Ryan V. Tappero,[‡] Kenneth J. Takeuchi,*[,†,§] Amy C. Marschilok,*[,†,§] and Esther S. Takeuchi*[,†,‡,§]

[†]Department of Chemistry, Stony Brook University, Stony Brook, New York 11794, United States

[‡]Brookhaven National Laboratory, Upton, New York 11973, United States

[§]Department of Materials Science and Engineering, Stony Brook University, Stony Brook, New York 11794, United States

ABSTRACT: Cathode solubility in batteries can lead to decreased and unpredictable long-term battery behavior due to transition metal deposition on the negative electrode such that it no longer supports high current. Analysis of negative electrodes from cells containing vanadium oxide or phosphorus oxide based cathode systems retrieved after long-term testing was conducted. This report demonstrates the use of synchrotron based X-ray microfluorescence (XRμF) to map negative battery electrodes in conjunction with microbeam X-ray absorption spectroscopy (μXAS) to determine the oxidation states of the metal centers resident in the solid electrolyte interphase (SEI) and at the electrode surface. Based on the empirical findings, a conceptual model for the location of metal ions in the SEI and their role in impacting lithium ion mobility at the electrode surfaces is proposed.

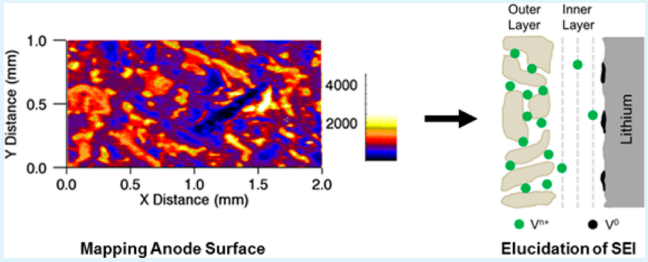

KEYWORDS: *silver vanadium oxide, silver vanadium phosphorus oxide, X-ray microfluorescence mapping, solid electrolyte interphase, lithium battery*

INTRODUCTION

Extended battery lifetime has increased significance with the prospect of long life applications such as electric vehicles and the integration of energy storage with the electric grid. Thus, consideration of parasitic reactions that occur over long periods of time has elevated significance. Characterization of electrode surfaces after long-term use has the potential to lend insight into mechanisms resulting in decreased performance. A life limiting mechanism for several battery systems is cathode solubility, resulting in formation of deposits on the anode surface, causing an increase in the cell impedance and resulting in loss of delivered capacity and capacity fade.[1] Manganese dissolution from cells using $LiMn_2O_4$ cathodes can exhibit long-term degradation of key performance metrics due to Mn dissolution,[1−7] resulting in deposition of Mn on the cell anode in the cell.[1,7−9] These deposited species increase the impedance of the electrode and result in capacity fade.[1] In a similar fashion, dissolution of vanadium is observed from discharged LiV_3O_8 material.[10−13] Cobalt dissolution from $LiCoO_2$ and subsequent deposition of Co on the negative electrode have been observed with direct correlation between capacity fade and cobalt deposition on the anode.[14−17] Thus, the dissolution of cathode materials into nonaqueous electrolytes and subsequent deposition on the negative electrode is an issue for many battery systems.

An important battery application demanding long life is the implantable cardiac defibrillator (ICD),[18−20] a growing application worldwide, with the US showing over 130 000 implants in the year 2011.[21] A metal oxide based battery system, lithium/silver vanadium oxide ($Ag_2V_4O_{11}$, SVO), is used to power these devices.[18] However, the battery has an unpredictable long-term stability limitation attributed to cathode material solubility, which results in deposits on the anode manifesting as increased battery resistance.[22,23] Although the reduction process of the cathode in the $Ag_2V_4O_{11}$ battery has been studied through characterization of the cathode material at various stages of discharge, analysis of the anode surface has not been reported.[24−26]

There are limited reports of negative electrodes analyses from cells including those containing manganese oxide cathodes.[27] Surface films containing manganese(II) were detected on graphite electrodes using electrolytes contaminated with manganese ions and were associated with a ∼15 times increase in the lithium-ion transfer resistance.[8,9] X-ray absorption near edge spectra (XANES) of lithium metal, lithium titanate, and graphite anodes from cycled cells with $LiMn_2O_4$ cathodes showed films containing manganese(II) and manganese metal were reported; however, locational information (i.e., mapping) was not available.[7,28] Detailed under-

Received: December 23, 2014
Accepted: February 17, 2015
Published: February 17, 2015

DOI: 10.1021/am509066n
ACS Appl. Mater. Interfaces 2015, 7, 5429−5437

standing of the location, composition, and role of the transition metal deposits on the negative electrode surfaces is lacking.

The study reported here investigates negative electrodes from cells subjected to long-term (~1 year rate) testing using cathodes containing metal oxide cathodes, specifically, silver vanadium oxide ($Ag_2V_4O_{11}$, SVO), or metal phosphate cathodes, specifically, silver vanadium phosphorus oxide ($Ag_2VO_2PO_4$, SVPO). Prior explorations of $Ag_2VO_2PO_4$ as a cathode material in lithium based batteries has demonstrated high discharge capacity and high current pulse capability[29−33] and yet lower solubility compared to silver vanadium oxide, $Ag_2V_4O_{11}$.[34−36] The lower solubility was predicted based on the hypothesis that phosphate based cathode materials reduce cathode component concentrations in the electrolyte, as the strong covalent P−O bonds from the inclusion of PO_4^{3-} polyanions stabilize the vanadium oxide framework.[37,38] Similar observations have been made on iron based systems where the phosphate based cathode material, $LiFePO_4$, provides higher stability in electrolyte relative to oxide based materials.[39,40] Thus, the silver vanadium phosphorus oxide and silver vanadium oxide cathode material systems are useful model systems for study as well as practically significant systems as the $Ag_2V_4O_{11}$ battery is in commercial use.

In this study, the negative electrodes of lithium/silver vanadium oxide and lithium/silver vanadium phosphorus oxide electrochemical cells were investigated by several techniques including mapping by synchrotron based X-ray microfluorescence (XRμF) and oxidation state determination by microbeam X-ray absorption spectroscopy (μXAS). Quantitative analysis of digested samples was done using inductively coupled plasma-optical emission spectroscopy (ICP-OES). These methods enabled visualization of the anode surface and solid electrolyte interphase (SEI) through mapping, determination of the vanadium oxidation state, and quantification of the silver and vanadium content of the recovered anodes. The findings indicate significant differences for the anode surfaces from the two cell types based on oxide versus phosphate based cathodes, clearly demonstrating lower deposition on the anode from the $Ag_2VO_2PO_4$ cells. This observation was considered in light of the improved long-term electrochemical performance to propose a conceptual model of the location and role of the metal ions deposited at the negative electrode. Because the X-ray microfluorescence technique described in the paper is ex situ and the data is collected when the Li anode is no longer immersed in electrolyte, we expect that the technique described is fully transferrable for investigating the SEI formation of other battery systems utilizing various electrolytes. Thus, from this study arises a paradigm to investigate use based performance degradation in battery systems through elucidation of the composition and geography of the negative electrode surface and SEI that will aid the broader community in more fully understanding this significant battery failure mechanism.

EXPERIMENTAL SECTION

Materials Synthesis and Characterization. Silver vanadium phosphorus oxide ($Ag_2VO_2PO_4$) was synthesized by a hydrothermal reaction according to a method previously reported in the literature using silver(I) oxide (Ag_2O), vanadium(V) oxide (V_2O_5), and phosphoric acid (H_3PO_4, 85%) as starting materials.[41] Silver vanadium oxide ($Ag_2V_4O_{11}$) was synthesized by a previously reported method.[42] Differential scanning calorimetry (DSC) analysis was performed using a TA Instruments Q20. Powder X-ray diffraction (XRD) measurements were recorded with a Rigaku Smart Lab X-ray diffractometer, using Cu Kα radiation and Bragg−Brentano focusing geometry.

Electrochemical Cell Assembly and Testing. Electrochemical tests were performed using coin-cell type experimental cells. Composite cathodes were prepared by mixing conductive carbon with silver vanadium phosphorus oxide or silver vanadium oxide with a composition of 85% active material and 15% graphite conductive additive. The anode was lithium foil and the electrolyte was 1 M $LiBF_4$ in propylene carbonate. All cells used two layers of Celgard 2500 separators, each of 25 μm thickness. The ratio of electrolyte to cathode material in the cells was 0.8. Constant current discharge and pulse discharge tests were performed at 37 °C. Commercially manufactured lithium silver vanadium oxide cells utilize 1 M $LiAsF_6$ salt in PC/DME electrolyte.[18,43−46] For this study, the 1 M $LiBF_4$ electrolyte system was chosen for this study, as it has been used previously as an electrolyte salt in studies investigating the Li/$Ag_2V_4O_{11}$ system.[47] We have previously tested and reported the solubility of the materials in $LiBF_4$/PC or $LiBF_4$/PC-DME electrolyte systems, and found that the presence of DME solvent insignificantly affects the material solubility.[34−36]

Treated lithium metal foil anodes were prepared by exposure to silver or vanadium containing solutions. ICP-OES of the treated anodes showed quantities of 14 and 21 $\mu g/cm^2$ for silver and vanadium, respectively. Electrochemical cells were constructed using one treated lithium as the working electrode and one fresh lithium foil as the counter electrode, each with an area of 1.6 cm^2. Control cells were constructed using fresh lithium for both electrodes. The AC impedance measurements were collected using a BioLogic VSP multichannel potentiostat with a 5 mV sinus amplitude over a frequency range of 10 mHz to 100 kHz. Analysis of AC impedance data was performed using ZView software, Version 3.3b where the data were fit to an equivalent circuit model to quantify the cell resistance.

Ex Situ Analysis. Post discharge, coin cells were disassembled under inert atmosphere. Disassembled anodes and cathodes were rinsed with a dimethyl carbonate solvent and dried under vacuum. Lithium anodes from $Ag_2V_4O_{11}$ and $Ag_2VO_2PO_4$ cells were prepared for analysis by X-ray microfluorescence, by transferring a portion of the anode to a sample holder with a beryllium window and an O-ring seal.

Synchrotron based X-ray microfluorescence (XRμF) images of lithium anodes recovered from the coin cells were acquired using Beamline X27A of the National Synchrotron Light Source (NSLS I) at Brookhaven National Laboratory (Upton, NY). This bend-magnet beamline uses Kirkpatrick−Baez (KB) mirrors to produce a focused spot (7 by 14 mm) of hard X-rays with tunable energy achieved via Si(111) or Si(311) channel-cut monochromator crystals.[48] For mSXRF imaging, the Si(111) monochromator was calibrated using a vanadium(V) metal foil and set to a fixed energy of 5.5 keV to excite the V K-edge. Samples were contained in a custom environmental cell with inert atmosphere and Be window. Samples were oriented 45° to the incident beam and rastered in the path of the beam by an XY stage while X-ray fluorescence was detected with a 4-element Vortex Silicon Drift Detector (SDD) positioned at 90° to the incident beam. Typical elemental maps were collected from a 1 × 2 mm sample area using a step size of 8 μm and a transit time of 80 ms. In the pre-edge region from 5395.0 to 5455.0 eV, and the post edge region from 5496.0 to 5615.0 eV, the incident beam energy was scanned using 2.0 eV energy steps. Across the vanadium K-edge from 5455.5 to 5495.0 eV, the step size was decreased to 0.5 eV for enhanced resolution. Vanadium compounds of varying oxidation states were used as reference materials, specifically vanadium metal foil, V_2O_3, V_2O_4, and $Ag_2VO_2PO_4$. For microbeam vanadium K-edge X-ray absorption spectroscopy (μXAS) measurements, the incident beam energy was scanned across the vanadium K-edge using 0.5 eV energy steps. All fluorescence signals were normalized to changes in intensity of the X-ray beam (I_0). Data acquisition and visualization were performed using IDL based beamline software developed for NSLS Beamline X26A. XAS data analysis was performed using Athena.[49] Inductively coupled plasma-optical emission spectroscopy (ICP-OES) was used to quantify the amount of silver and vanadium on the lithium anodes by digestion

DOI: 10.1021/am509066n
ACS Appl. Mater. Interfaces 2015, 7, 5429−5437

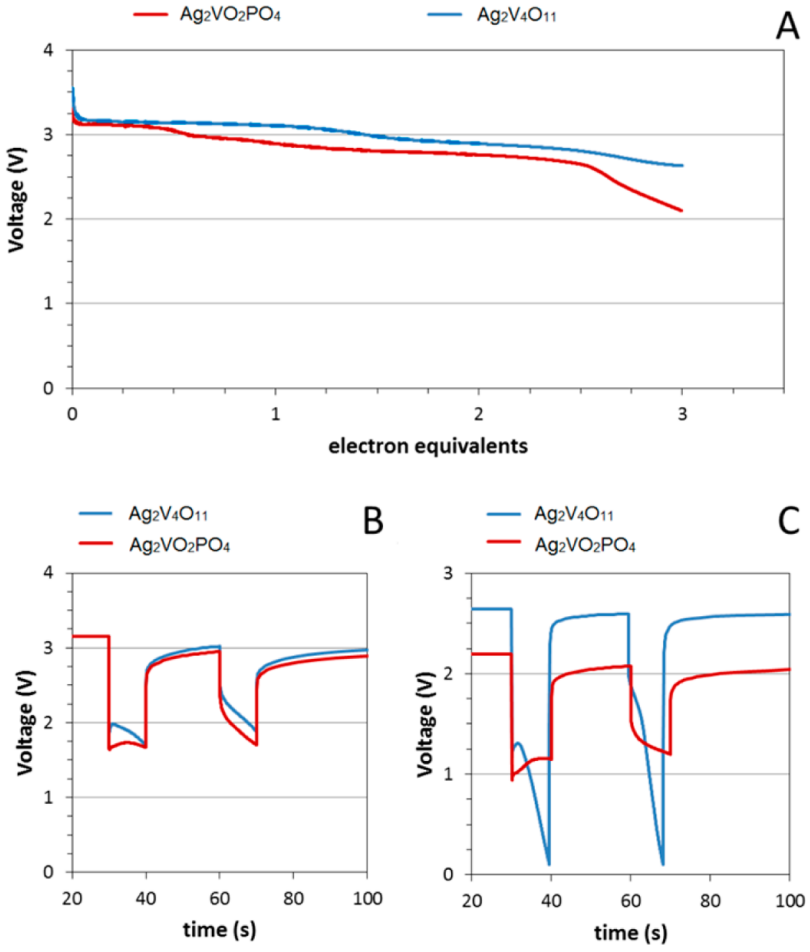

Figure 1. A. Long-term (~1 year rate) discharge for lithium anode cells containing silver vanadium oxide ($Ag_2V_4O_{11}$) and silver vanadium phosphorus oxide ($Ag_2VO_2PO_4$) cathodes. B. Voltage versus time for pulse discharge at 2 electron equivalents of discharge. C. Voltage versus time for pulse discharge at 3 electron equivalents of discharge.

in a nitric acid solution and subsequent analysis using a Thermofisher iCAP 6300 series ICP-OES.

RESULTS AND DISCUSSION

Materials and Characterization. Silver vanadium oxide ($Ag_2V_4O_{11}$, SVO) and silver vanadium phosphorus oxide ($Ag_2VO_2PO_4$, SVPO) materials were characterized using powder X-ray diffraction. The measured XRD pattern of $Ag_2VO_2PO_4$ compared well with the previously reported reference pattern (PDF # 01-081-2149).[50] $Ag_2VO_2PO_4$ crystallizes in monoclinic space group $C2/m$, with the structure characterized by layers of edge shared VO_6 octahedra and PO_4 tetraheda.[50] Silver ions are located between the layers, which run parallel to the (001) plane. The measured XRD pattern of $Ag_2V_4O_{11}$ was matched to reference pattern PDF# 01-070-7658.[51] $Ag_2V_4O_{11}$ also crystallizes in a layered structure with space group $C2/m$. Edge and corner sharing VO_6 octahedra form layers that stack in the [001] direction, with silver ions between the layers. Differential scanning calorimetry was used to confirm the phase purity of both materials. Surface areas measured using the Brunauer–Emmett–Teller (BET) technique were 1.1 ± 0.1 and 0.9 ± 0.1 for $Ag_2VO_2PO_4$ and $Ag_2V_4O_{11}$, respectively.

Electrochemical Testing. After synthesis and confirmation of the structure of silver vanadium oxide ($Ag_2V_4O_{11}$, SVO), and silver vanadium phosphorus oxide ($Ag_2VO_2PO_4$, SVPO), the materials were used as cathodes in lithium metal anode coin cells. Cells were discharged at 37 °C under constant current over 100 or 150 days to 2 or 3 electron equivalents, respectively (Figure 1A.) The current was adjusted to keep the time the same for both sets of cells where currents of 7.9×10^{-6} A for the SVO ($Ag_2V_4O_{11}$) cells and 1.18×10^{-5} A for the SVPO ($Ag_2VO_2PO_4$) cells were used. Discharge levels of 2 and 3 electron equivalents were selected for both systems, as the silver content in each formula is Ag_2. Silver vanadium phosphorus oxide was reduced to 50% and 75% depth of discharge, and silver vanadium oxide was reduced 28.5% and 42.8% depth of discharge. Discharge was done slowly to mimic long-term use in patients where the ICD devices would be powering background functions. This allows probing of low levels of cathode dissolution and subsequent deposition of silver and vanadium from the cathode materials onto the lithium anode surfaces. After the cells attained the targeted level of discharge, constant current pulses were applied to the cells to simulate intermittent therapy delivery of an ICD. One cell at each condition was pulse tested where two 10 s, 20 mA/cm^2 pulses were applied with a 20 s rest period between pulses. The voltage versus time response is shown in Figure 1B,C. After reduction by 2 electron equivalents, comparable performance was seen for the $Ag_2V_4O_{11}$ and $Ag_2VO_2PO_4$ cells where both cells could sustain pulse voltages above 1.5 V, Figure 1B. Pulse testing after 3 electron equivalents of reduction showed that the

DOI: 10.1021/am509066n
ACS Appl. Mater. Interfaces 2015, 7, 5429–5437

$Ag_2VO_2PO_4$ cells displayed a small amount of voltage delay where the leading edge of the voltage under pulse was lower (~1.0 V) than the 10 s point of the pulse (~1.1 V), Figure 1C. The minimum voltage under the second pulse was higher at 1.2 V. In contrast, the $Ag_2V_4O_{11}$ cell discharged to 3 electron equivalents exhibited significant polarization upon pulsing. Although there was some amount of voltage delay as the leading edge of the pulse dropped to 0.9 V and recovered slightly, the pulse voltage then dropped sharply as the pulse continued to a minimum voltage of ~0.1 V. The second pulse could not deliver useful power as the voltage under the second pulse dropped to ~0.1 V as well.

The DC resistance (R_{DC}) for the four pulse discharged cells was calculated. and the results are tabulated in Table 1. The

Table 1. Calculated Direct Current Resistance (R_{DC}) for Li/$Ag_2VO_2PO_4$ and Li/$Ag_2V_4O_{11}$ Cells under Pulse Discharge at 2 and 3 Electron Equivalents

		R_{DC} (Ω)	
cell type	electron equivalents	Pulse 1	Pulse 2
Li/$Ag_2VO_2PO_4$	2	56	46
	3	39	32
Li/$Ag_2V_4O_{11}$	2	55	43
	3	95	93

R_{DC} of the $Ag_2V_4O_{11}$ and $Ag_2VO_2PO_4$ cells were comparable after discharge to 2 electron equivalents, but after discharge to 3 electron equivalents, the R_{DC} of the $Ag_2V_4O_{11}$ cell was approximately 2× that of the $Ag_2VO_2PO_4$ cell. In practical device terms, appropriately designed cells based on $Ag_2VO_2PO_4$ or $Ag_2V_4O_{11}$ could successfully deliver sufficient energy, ~30 J, to deliver therapy in an ICD after discharge equivalent to 2 electrons. However, after 3 electrons of discharge, the $Ag_2V_4O_{11}$ would no longer be able to support delivery of a therapy pulse. The electrochemical results affirm that after slow discharge to 3 electron equivalents, cells with $Ag_2VO_2PO_4$ cathodes can sustain significantly higher pulse voltage than $Ag_2V_4O_{11}$ cells. These results motivated studies of the cell components, in particular the cell anodes, to determine if a correlation between the anode surface composition and electrochemical performance could be established.

Ex Situ Cathode Characterization. Post discharge, cell cathodes were recovered and analyzed by X-ray powder diffraction. XRD patterns indicated the presence of silver metal for both cathode materials discharged to two and three electron equivalents. The integrated area of the silver peak at 44.2° 2θ is higher for the $Ag_2VO_2PO_4$ (6000 and 6500 at 2 and 3 electron reduction, respectively) material compared to $Ag_2V_4O_{11}$ (3800 and 4100 at 2 and 3 electron reduction, respectively), indicating slightly higher levels of reduced silver in the $Ag_2VO_2PO_4$ cathode. As has been previously reported for silver−vanadium bimetallic materials, some vanadium reduction takes place in parallel with the reduction of silver.[25,31−33,52] Previous studies of discharged $Ag_2V_4O_{11}$[25,26] indicate that vanadium oxidation states of V, IV, and III can coexist once the material is discharged past 2 electron equivalents. For $Ag_2VO_2PO_4$, a recent X-ray absorption spectroscopy study[31] has shown that the vanadium is present as a mixture of oxidation states IV and III when the material is discharged to 3 electron equivalents. Thus, both oxidation states of IV and III are expected to be present in $Ag_2V_4O_{11}$ and $Ag_2VO_2PO_4$ cathode materials when discharged to 3 electron equivalents.

Ex Situ Lithium Anode Characterization: X-ray Microfluorescence. Vanadium K-edge elemental maps of anodes from cells discharged to 2 electron equivalents are shown in Figure 2A,B for the anodes from the $Ag_2V_4O_{11}$ and $Ag_2VO_2PO_4$ cells, respectively. Within the 1 × 1 mm area analyzed, the anodes from the $Ag_2V_4O_{11}$ cell and the $Ag_2VO_2PO_4$ cell appear relatively similar. There are some areas of higher and lower vanadium intensity visible, likely a result of some surface roughness of the partially discharged lithium surface. Experiments on lithium stripping in carbonate based electrolytes have indicated that the lithium surface is locally dissolved to form a randomized, pitted surface due to areas of passivation film breakdown.[53] Thus, some regions of the electrode may have thicker regions of SEI where higher amounts of V are expected. Vanadium K-edge elemental maps of anodes from cells discharged to 3 electron equivalents were recorded and are shown in Figure 2C,D for the anodes from the $Ag_2V_4O_{11}$ and $Ag_2VO_2PO_4$ cells, respectively. Contrary to the anodes from the cells depleted by 2 electrons, the anodes from the $Ag_2V_4O_{11}$ and $Ag_2VO_2PO_4$ cells are different in appearance. Within the 1 × 2 mm area analyzed, the anode from the $Ag_2V_4O_{11}$ cell exhibits large and distinct areas of much higher intensity of the

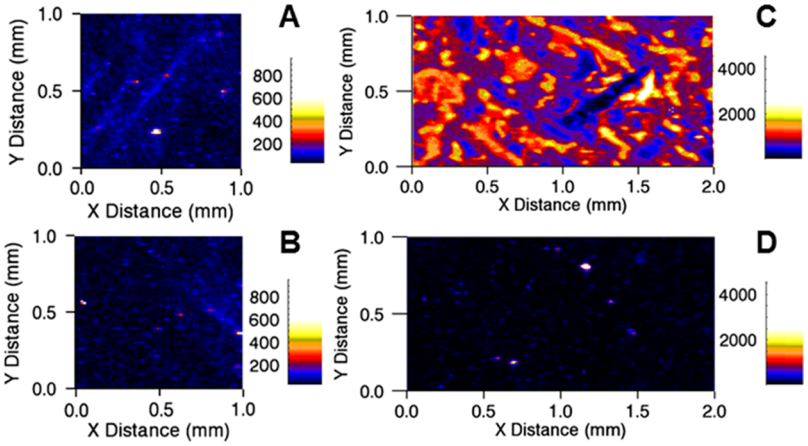

Figure 2. Vanadium elemental maps of anodes from A. Li/$Ag_2V_4O_{11}$ cell discharged to 2 electron equivalents. B. Li/$Ag_2VO_2PO_4$ cell discharged to 2 electron equivalents. C. Li/$Ag_2V_4O_{11}$ cell discharged to 3 electron equivalents. D. Li/$Ag_2VO_2PO_4$ cell discharged to 3 electron equivalents.

DOI: 10.1021/am509066n
ACS Appl. Mater. Interfaces 2015, 7, 5429−5437

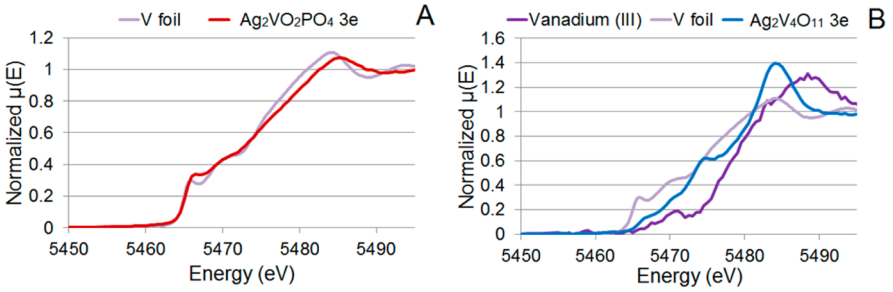

Figure 3. A. XANES spectra from lithium surface of $Ag_2VO_2PO_4$ 3 electron equivalent cell at a region of high intensity, overlaid with the vanadium foil (V^0) standard. B. XANES spectra from lithium surface of $Ag_2V_4O_{11}$ 3 electron equivalent cell overlaid with vanadium(III) ion (V^{3+}) and vanadium foil (V^0) standards.

vanadium signal. In contrast, the anode from the $Ag_2VO_2PO_4$ cell exhibited low vanadium signal intensity for the majority of the analyzed area, with a few small localized regions of high intensity, illustrating differences in the vanadium content over the lithium surface.

The result of the X-ray microfluorescence (XRμF) can be considered in conjunction with the pulse discharge data. A previous study reported lithium metal surfaces treated with electrolyte containing dissolved vanadium significantly increased the impedance of a cell.[35] From those results, it would be reasonable to expect that the cells displaying low pulse voltage and high resistance would have higher levels of vanadium deposited on the lithium anode surfaces. For the lithium anodes from the $Ag_2V_4O_{11}$ and $Ag_2VO_2PO_4$ cells analyzed as part of this study, the vanadium detected after 2 electrons of reduction are generally low. Additionally, the vanadium detected on the lithium anode from the $Ag_2VO_2PO_4$ cell after 3 electrons of reduction is also generally low. In sharp contrast, the lithium anode from the $Ag_2V_4O_{11}$ cell discharged to 3 electrons shows much higher levels of vanadium present, consistent with the large voltage drop observed during the pulse discharge test.

Microbeam X-ray absorption spectroscopy (μXAS) measurements made in the vanadium K-edge XANES region were collected at various positions for the elemental maps of the anodes to interrogate the nature of the vanadium species deposited on the anode surface. For the $Ag_2VO_2PO_4$ 3 electron discharged cell, XANES spectra collected at positions on the elemental map exhibiting low vanadium K-edge signal intensity exhibited low signal-to-noise due to the small amount of vanadium present on the surface. In areas with very low levels of vanadium, the signal intensity was low, but the vanadium species indicate an average oxidation state between I and III. Spectra collected at the highest intensity region on the map, at $x = 1.2$, $y = 0.8$, are plotted and overlaid with the vanadium foil spectrum, Figure 3A. The similarity in edge position and profile of the sample and the reference foil suggests that the vanadium deposited on the lithium anode surface in this localized region was reduced to vanadium metal. Comparable spectra were also collected at the higher intensity region $x = 1.5$, $y = 0.9$. These data provide evidence that the vanadium species on the anode from the $Ag_2VO_2PO_4$ cell showing highest intensity are vanadium metal.

XANES data collected at various positions for the anodes from the $Ag_2V_4O_{11}$ cells discharged to 3 electron equivalents show similar spectra. A representative XANES spectrum for the 3 electron $Ag_2V_4O_{11}$ anode sample collected at location $x = 1.0$, $y = 0.5$ is overlaid with the vanadium standards, Figure 3B. The vanadium K-edge of the sample spectrum is positioned at an energy between the K-edge for the vanadium(0) and vanadium(III) standards, suggesting that the vanadium species deposited on the anode are not fully reduced to vanadium metal and that more than a single vanadium oxidation state may be present. Further, the general profile of the sample spectra differ from those of the reference materials suggesting that the chemistry of deposited vanadium species is different from the vanadium foil and oxide reference materials.

The XANES data indicate that there are some differences in the overall vanadium species deposited on the lithium anode in the $Ag_2V_4O_{11}$ cell compared to the anode in the $Ag_2VO_2PO_4$ cell. For the anode recovered from the $Ag_2V_4O_{11}$ cell after 3 electrons, the data suggests that the average oxidation state of the vanadium species on the surface is between III and 0, not fully reduced to vanadium metal. The anode from the $Ag_2VO_2PO_4$ cell shows that there are localized areas of high concentration vanadium that are fully reduced to vanadium metal. Measurement of the lithium surfaces remote from the areas of high concentration showed little vanadium present, with average oxidation states between I and III.

The results of these findings can be rationalized as follows. Multiple oxidation states of vanadium may be present in solution including vanadium(V), vanadium(IV), and vanadium(III). As the vanadium centers approach the lithium surface, the vanadium species will encounter the solid electrolyte interphase (SEI) at the lithium surface. Based on the difference in standard reduction potentials of vanadium and lithium, at lithium potential, the vanadium ions may be reduced with some reduced to vanadium metal. The data indicate that some of the vanadium detectable on the anode surface is not fully reduced to vanadium metal. Thus, consideration of the nature of the SEI is warranted. The SEI can be viewed as having two layers where the outer layer is porous and has significant organic content and the inner denser layer is considered to have significant inorganic content. Notably, two differing mechanisms have been proposed for ion migration through the layers where lithium ions diffuse via pore diffusion through the outer layer and a knock-off mechanism through the inner dense layer.[54,55] Thus, migration of the charged vanadium species through the SEI may take place under two regimes. The vanadium ions more readily diffuse through the more porous outer SEI layer, yet diffuse slowly through the inner layer. In the case of the anodes from the $Ag_2VO_2PO_4$ cells, low levels of charged vanadium are detectable across the surface of the anode consistent with the migration of the species through the electrolyte and into the porous layer of the SEI. There are some localized areas where the vanadium is fully reduced to vanadium metal indicating that the vanadium species migrated successfully through the inner SEI on a limited basis to reach

DOI: 10.1021/am509066n
ACS Appl. Mater. Interfaces 2015, 7, 5429−5437

the lithium surface and are reduced to vanadium metal. This is schematically depicted in Figure 4.

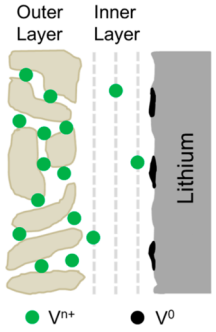

Figure 4. Schematic of lithium anode surface including solid electrolyte interphase (SEI) indicating location of positively charged vanadium ions, V^{n+}, and vanadium metal, V^0.

The anodes from the $Ag_2V_4O_{11}$ cells show an average oxidation state from the XANES data between vanadium(0) and vanadium(III) for the entire surface. In the case of the anode from the $Ag_2V_4O_{11}$ cell where significant amounts of vanadium are in solution, much of the vanadium found on the anode surface has not fully migrated through the SEI and reduced to vanadium metal, but has heavily loaded the porous outer layer of the SEI. The inner layer would also be expected to contain some vanadium in more limited amounts. It is reasonable to project that the presence of these positively charged vanadium species in the SEI may inhibit facile movement of the positively charged lithium ions. This supports the strong correlation of the poor pulse discharge results with the level of vanadium on the surface as observed with the $Ag_2V_4O_{11}$ cell discharged to 3 electron equivalents. The results also provide insight into the kinetic behavior of the various steps in the process. The data imply that vanadium dissolution and migration to the anode is a relatively fast process as is the migration of the vanadium cations into the outer layer of the SEI when compared to the slower migration of the charged vanadium ions through the dense inner layer of the SEI.

Quantitative Analysis of Anodes. Subsequent to the X-ray microfluorescence (XRμF) experiment, lithium anodes recovered from the cells were digested and quantitatively analyzed by ICP-OES to determine the levels of silver and vanadium present. Figure 5A,B shows the results of the ICP-OES analysis for silver and vanadium, respectively. Silver and vanadium dissolution from $Ag_2V_4O_{11}$ and $Ag_2VO_2PO_4$ materials in electrolyte solutions have been previously quantified for the unreduced materials.[35,36]

The concentration of silver deposited onto the anode surfaces ranged from 2.7 to 6.5 $\mu g/cm^2$. The anodes recovered from the $Ag_2VO_2PO_4$ cells showed slightly higher amounts of silver than those from the $Ag_2V_4O_{11}$ cells after 2 electrons of reduction. After 3 electrons, the trend reversed where the anodes from the $Ag_2V_4O_{11}$ cells showed slightly higher levels of silver; however, in both cases, the differences are relatively small. Analysis of the vanadium deposited onto the lithium anodes by ICP-OES indicated similar levels of deposition for the 2 and 3 electron equivalent reduced $Ag_2VO_2PO_4$ cells and the 2 electron equivalent reduced $Ag_2V_4O_{11}$ cells where the values ranged from 0.3 to 1.2 $\mu g/cm^2$. In contrast, anodes from the $Ag_2V_4O_{11}$ cells discharged to 3 electron equivalents exhibited a higher level of vanadium deposition, where individual anodes had vanadium surface concentrations of 3.3 and 3.4 $\mu g/cm^2$, higher by a factor of $\geq$3×. It is notable that the levels of silver deposition onto the anode surface are higher than that of vanadium consistent with previous reports of dissolution from the nondischarged materials where silver dissolution levels through 3-weeks was approximately 2× and 7× that of vanadium for $Ag_2V_4O_{11}$ and $Ag_2VO_2PO_4$, respectively.[35,36]

Higher levels of vanadium dissolution are observed for the Li/$Ag_2V_4O_{11}$ cells discharged to 3 electron equivalents. At this depth of discharge, multiple vanadium oxidation states of V, IV, and III may be present.[25,26] Limited literature exists regarding the influence of vanadium oxidation state on solubility.[56] In aqueous solution, V(V) forms oxyanions such as $H_nVO_4^{n-3}$, V(IV) is primarily present as vanadyl, VO^{2+}, while V(III) forms vanadium hydroxide, $V(OH)_3$.[57] The highly ionic V(IV) and V(V) species are reported to be more soluble than V(III) in aqueous media.[57] Because solubility is a function of both lattice energy and solvation energy, it can be proposed that in aqueous solution, the hydration energies associated with higher oxidation states of vanadium can overcome the associated lattice energies, resulting in enhanced dissolution of higher oxidations states of vanadium. Conversely, in nonaqueous solutions where the polarity of the solvent is reduced, the solvation energies are expected to be much lower than the corresponding lattice energies for high oxidation states of vanadium. However, for V(III), the solvation energy may be able to compete with the reduced lattice energy, resulting in increased dissolution for V(III) relative to V(V) in nonaqueous solution. Thus, in nonaqueous electrolyte, dissolution may become more favorable for discharged $Ag_2V_4O_{11}$ oxide material reduced by 3 electron equivalents that contains V(III) metal centers. Notably, the low vanadium oxidation state of the discharged $Ag_2VO_2PO_4$ material reduced by 3 electron equivalents does not result in significantly higher solubility, consistent with our hypothesis that the strong covalent P−O bonds from the inclusion of PO_4^{3-} polyanions would stabilize the vanadium oxide framework, regardless of vanadium oxidation state.

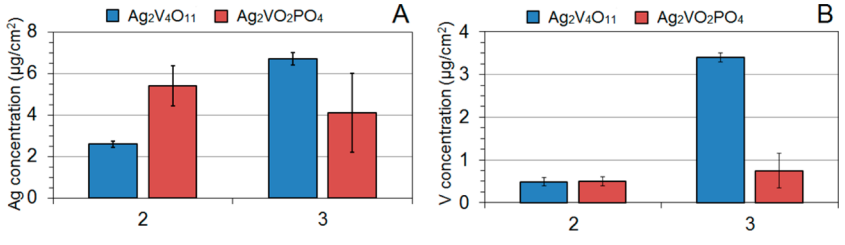

Figure 5. Quantitative analysis of lithium anodes recovered from $Ag_2V_4O_{11}$ and $Ag_2VO_2PO_4$ cathode cells discharged to 2 and 3 electron equivalents for A. silver (Ag) and B. vanadium (V).

DOI: 10.1021/am509066n
ACS Appl. Mater. Interfaces 2015, 7, 5429−5437

To further elucidate the role of vanadium and silver on the surface of a lithium anode, lithium anodes were surface treated by immersion in silver ion and vanadium ion containing solutions. Post treatment, the anodes were used for impedance studies that revealed that silver treatment of the anode does not increase the impedance of the system whereas the vanadium-treated samples displayed higher impedance, Figure 6. The

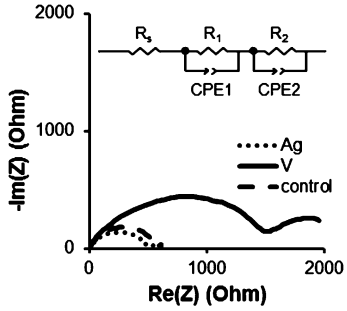

Figure 6. AC impedance results plotted in Nyquist format for lithium/lithium cells showing untreated, silver (Ag)-treated and vanadium (V)-treated samples. Inset shows equivalent circuit used for analysis.

equivalent circuit analysis yielded R_{total} values of 570, 487, and 1538 Ω for the untreated, silver-treated, and vanadium-treated anodes, respectively. Increased cell resistance with accompanying voltage drop under pulse for the vanadium-treated anodes has been previously reported.[35] Thus, this work focuses on vanadium deposition on the anode where the impedance was demonstrated to change in contrast to the silver deposition, which does not contribute to increased cell resistance.[36] These results highlight the complex nature of the SEI where composition is critical to the resultant impedance of the electrode.

CONCLUSION

Based on the data, a conceptual model for the interaction of the charged vanadium species and the SEI at the anode of lithium/silver vanadium oxide and lithium/silver vanadium phosphorus oxide batteries is proposed. The soluble vanadium ions migrate through the electrolyte and penetrate the pores of the outer layer of the SEI where the vanadium ions maintain a positive charge. More slowly, some vanadium ions reach the lithium surface with some reduced to vanadium metal. There is a strong correlation with the observed increase in battery resistance and the presence of vanadium on the surfaces of the anodes and vanadium cations in the SEI layer. It is reasonable to project that (1) the presence of metallic vanadium on the lithium anode surface would significantly reduce usable current, and (2) vanadium cations within the SEI may inhibit facile movement of the positively charged lithium ions. These findings shed light on the nature and composition of the anode solid electrolyte interphase (SEI) and further highlight its importance in understanding and predicting decreases in battery performance. Further, the findings indicate significant differences for the anode surfaces recovered from the $Ag_2V_4O_{11}$ and $Ag_2VO_2PO_4$ cell types, and are conceptually summarized in Figure 7. The results clearly support that $Ag_2VO_2PO_4$ cathode material provides the opportunity for future development of ICD batteries with improved charge time stability under long-term use. Finally, the strategy presented for analysis of anodes from the $Ag_2V_4O_{11}$ and $Ag_2VO_2PO_4$ cell systems could be extended to systems with cathodes of other metallic compositions; thus

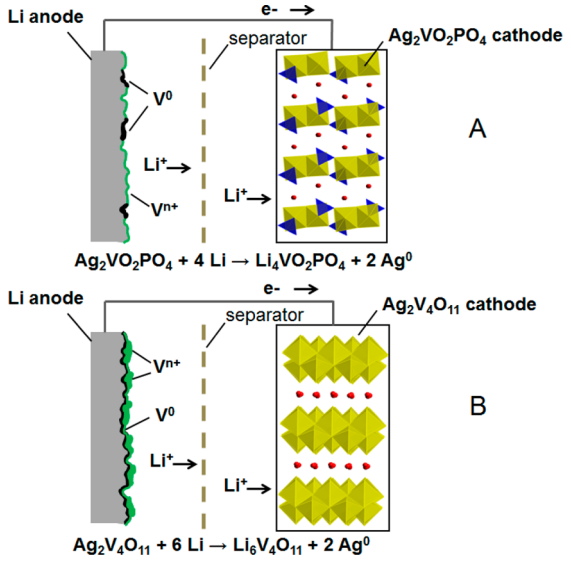

Figure 7. Schematic cell representations of indicating deposition of vanadium species on the anode surfaces for A. lithium/silver vanadium phosphorus oxide ($Li/Ag_2VO_2PO_4$) cell, and B. lithium/silver vanadium oxide ($Li/Ag_2V_4O_{11}$) cell.

by analogy, we propose a new paradigm for probing a critical long-term failure mode for a number of battery systems.

AUTHOR INFORMATION

Corresponding Authors

*K. J. Takeuchi. Email: kenneth.takeuchi.1@stonybrook.edu.
*A. C. Marschilok. Email: amy.marschilok@stonybrook.edu.
*E. S. Takeuchi. Email: esther.takeuchi@stonybrook.edu.

Notes

The authors declare no competing financial interest.

ACKNOWLEDGMENTS

The synthesis, characterization, and pulse discharge studies were supported by the National Institutes of Health under Grant 1R01HL093044-01A1 from the National Heart, Lung, and Blood Institute. Mechanistic investigation of the material via XRF was supported by the Department of Energy, Office of Basic Energy Sciences. Portions of this work were performed at Beamline X27A, National Synchrotron Light Source (NSLS), Brookhaven National Laboratory (BNL). X27A is supported in part by DOE- Geosciences (DE-FG02-92ER14244 to The University of Chicago-CARS). Use of NSLS I was supported by the DOE under Contract No. DE-AC02-98CH10886. The authors acknowledge Jurgen Thieme and Paul Northrup for helpful discussions relevant to the XRF experiments. Development of the experimental methodology for XRF measurement was supported by the U.S. Department of Energy, Office of Science, Office of Basic Energy Sciences, under Contract No. DE-AC02-98CH10886.

REFERENCES

(1) Vetter, J.; Novak, P.; Wagner, M. R.; Veit, C.; Moeller, K. C.; Besenhard, J. O.; Winter, M.; Wohlfahrt-Mehrens, M.; Vogler, C.; Hammouche, A. Ageing Mechanisms in Lithium-Ion Batteries. *J. Power Sources* **2005**, *147*, 269−281.

(2) Jang, D. H.; Shin, Y. J.; Oh, S. M. Dissolution of Spinel Oxides and Capacity Losses in 4 V $Li/Li_xMn_2O_4$ Cells. *J. Electrochem. Soc.* **1996**, *143*, 2204−2211.

DOI: 10.1021/am509066n
ACS Appl. Mater. Interfaces 2015, 7, 5429−5437

(3) Jang, D. H.; Oh, S. M. Electrolyte Effects on Spinel Dissolution and Cathodic Capacity Losses in 4 V $Li/Li_xMn_2O_4$ Rechargeable Cells. *J. Electrochem. Soc.* **1997**, *144*, 3342−3348.
(4) Blyr, A.; Sigala, C.; Amatucci, G.; Guyomard, D.; Chabre, G. Y.; Tarascon, J. M. Self-Discharge of $LiMn_2O_4$/C Li-Ion Cells in Their Discharged State. Understanding by Means of Three-Electrode Measurements. *J. Electrochem. Soc.* **1998**, *145*, 194−209.
(5) du Pasquier, A.; Blyr, A.; Courjal, P.; Larcher, D.; Amatucci, G.; Gerand, B.; Tarascon, J. M. Mechanism for Limited 55°C Storage Performance of $Li_{1.05}Mn_{1.95}O_4$ Electrodes. *J. Electrochem. Soc.* **1999**, *146*, 428−436.
(6) Lu, C.-H.; Lin, S.-W. Dissolution Kinetics of Spinel Lithium Manganate and Its Relation to Capacity Fading in Lithium Ion Batteries. *J. Mater. Res.* **2002**, *17*, 1476−1481.
(7) Zhan, C.; Lu, J.; Kropf, A. J.; Wu, T.; Jansen, A. N.; Sun, Y.-K.; Qiu, X.; Amine, K. Mn(II) Deposition on Anodes and Its Effects on Capacity Fade in Spinel Lithium Manganate-Carbon Systems. *Nat. Commun.* **2013**, *4*, Article No. 2437, 8 pp.
(8) Ochida, M.; Domi, Y.; Doi, T.; Tsubouchi, S.; Nakagawa, H.; Yamanaka, T.; Abe, T.; Ogumi, Z. Influence of Manganese Dissolution on the Degradation of Surface Films on Edge Plane Graphite Negative-Electrodes in Lithium-Ion Batteries. *J. Electrochem. Soc.* **2012**, *159*, A961−A966.
(9) Delacourt, C.; Kwong, A.; Liu, X.; Qiao, R.; Yang, W. L.; Lu, P.; Harris, S. J.; Srinivasan, V. Effect of Manganese Contamination on the Solid-Electrolyte-Interphase Properties in Li-Ion Batteries. *J. Electrochem. Soc.* **2013**, *160*, A1099−A1107.
(10) Jouanneau, S.; Le, G. L. S. A.; Verbaere, A.; Guyomard, D. The Origin of Capacity Fading Upon Lithium Cycling in $Li_{1.1}V_3O_8$. *J. Electrochem. Soc.* **2005**, *152*, A1660−A1667.
(11) Jouanneau, S.; Verbaere, A.; Lascaud, S.; Guyomard, D. Improvement of the Lithium Insertion Properties of $Li_{1.1}V_3O_8$. *Solid State Ionics* **2006**, *177*, 311−315.
(12) Gao, X.-W.; Wang, J.-Z.; Chou, S.-L.; Liu, H.-K. Synthesis and Electrochemical Performance of LiV_3O_8/Polyaniline as Cathode Material for the Lithium Battery. *J. Power Sources* **2012**, *220*, 47−53.
(13) Shi, Q.; Hu, R.; Zeng, M.; Dai, M.; Zhu, M. The Cycle Performance and Capacity Fading Mechanism of a LiV_3O_8 Thin-Film Electrode with a Mixed Amorphous-Nanocrystalline Microstructure. *Electrochim. Acta* **2011**, *56*, 9329−9336.
(14) Amatucci, G. G.; Tarascon, J. M.; Klein, L. C. Cobalt Dissolution in $LiCoO_2$-based Non-aqueous Rechargeable Batteries. *Solid State Ionics* **1996**, *83*, 167−173.
(15) Aurbach, D.; Markovsky, B.; Rodkin, A.; Levi, E.; Cohen, Y. S.; Kim, H. J.; Schmidt, M. On the Capacity Fading of $LiCoO_2$ Intercalation Electrodes: The Effect of Cycling, Storage, Temperature, and Surface Film Forming Additives. *Electrochim. Acta* **2002**, *47*, 4291−4306.
(16) Markevich, E.; Salitra, G.; Aurbach, D. Influence of the PVDF Binder on the Stability of $LiCoO_2$ Electrodes. *Electrochem. Commun.* **2005**, *7*, 1298−1304.
(17) Aurbach, D.; Markovsky, B.; Salitra, G.; Markevich, E.; Talyossef, Y.; Koltypin, M.; Nazar, L.; Ellis, B.; Kovacheva, D. Review on Electrode-Electrolyte Solution Interactions, Related to Cathode Materials for Li-Ion Batteries. *J. Power Sources* **2007**, *165*, 491−499.
(18) Bock, D. C.; Marschilok, A. C.; Takeuchi, K. J.; Takeuchi, E. S. Batteries Used to Power Implantable Biomedical Devices. *Electrochim. Acta* **2012**, *84*, 155−164.
(19) Takeuchi, E. S.; Quattrini, P. J.; Greatbatch, W. Lithium/Silver Vanadium Oxide Batteries for Implantable Defibrillators. *Pacing Clin. Electrophysiol.* **1988**, *11*, 2035−2039.
(20) Takeuchi, K. J.; Marschilok, A. C.; Davis, S. M.; Leising, R. A.; Takeuchi, E. S. Silver Vanadium Oxides and Related Battery Applications. *Coord. Chem. Rev.* **2001**, *219−221*, 283−310.
(21) Mond, H. G.; Proclemer, A. The 11th World Survey of Cardiac Pacing and Implantable Cardioverter-Defibrillators: Calendar Year 2009—A World Society of Arrhythmia's Project. *Pacing Clin. Electrophysiol.* **2011**, *34*, 1013−1027.
(22) Yumoto, H.;Tan, T.; Piao, T.; Tsukamoto, H.; Koel, B. Talk #532 - Silver and Vanadium Dissolution in Li/SVO Primary Batteries. *206th Meeting of the Electrochemical Society. Session C1 - Battery and Energy Technology Joint General Session*, Honolulu, Hawaii, October 6, 2004.
(23) Root, M. J. Resistance Model for Lithium-Silver Vanadium Oxide Cells. *J. Electrochem. Soc.* **2011**, *158*, A1347−A1353.
(24) Takeuchi, E. S.; Thiebolt, W. C., III The Reduction of Silver Vanadium Oxide in Lithium/Silver Vanadium Oxide Cells. *J. Electrochem. Soc.* **1988**, *135*, 2691−2694.
(25) Leising, R. A.; Thiebolt, W. C., III; Takeuchi, E. S. Solid-State Characterization of Reduced Silver Vanadium Oxide from the Li/SVO Discharge Reaction. *Inorg. Chem.* **1994**, *33*, 5733−5740.
(26) Leifer, N. D.; Colon, A.; Martocci, K.; Greenbaum, S. G.; Alamgir, F. M.; Reddy, T. B.; Gleason, N. R.; Leising, R. A.; Takeuchi, E. S. Nuclear Magnetic Resonance and X-ray Absorption Spectroscopic Studies of Lithium Insertion in Silver Vanadium Oxide Cathodes. *J. Electrochem. Soc.* **2007**, *154*, A500−A506.
(27) Yang, L.; Takahashi, M.; Wang, B. A Study on Capacity Fading of Lithium-Ion Battery with Manganese Spinel Positive Electrode During Cycling. *Electrochim. Acta* **2006**, *51*, 3228−3234.
(28) Gowda, S. R.; Gallagher, K. G.; Croy, J. R.; Bettge, M.; Thackeray, M. M.; Balasubramanian, M. Oxidation State of Cross-over Manganese Species on the Graphite Electrode of Lithium-Ion Cells. *Phys. Chem. Chem. Phys.* **2014**, *16*, 6898−6902.
(29) Marschilok, A. C.; Takeuchi, K. J.; Takeuchi, E. S. Preparation and Electrochemistry of Silver Vanadium Phosphorous Oxide, $Ag_2VO_2PO_4$. *Electrochem. Solid-State Lett.* **2008**, *12*, A5−A9.
(30) Kim, Y. J.; Lee, C.-Y.; Marschilok, A. C.; Takeuchi, K. J.; Takeuchi, E. S. Ag_xVOPO_4: A Demonstration of the Dependence of Battery-Related Electrochemical Properties of Silver Vanadium Phosphorous Oxides on Ag/V Ratios. *J. Power Sources* **2011**, *196*, 3325−3330.
(31) Patridge, C. J.; Jaye, C.; Abtew, T. A.; Ravel, B.; Fischer, D. A.; Marschilok, A. C.; Zhang, P.; Takeuchi, K. J.; Takeuchi, E. S.; Banerjee, S. An X-ray Absorption Spectroscopy Study of the Cathodic Discharge of $Ag_2VO_2PO_4$: Geometric and Electronic Structure Characterization of Intermediate Phases and Mechanistic Insights. *J. Phys. Chem. C* **2011**, *115*, 14437−14447.
(32) Marschilok, A. C.; Kozarsky, E. S.; Tanzil, K.; Zhu, S.; Takeuchi, K. J.; Takeuchi, E. S. Electrochemical Reduction of Silver Vanadium Phosphorous Oxide, $Ag_2VO_2PO_4$: Silver Metal Deposition and Associated Increase in Electrical Conductivity. *J. Power Sources* **2010**, *195*, 6839−6846.
(33) Takeuchi, E. S.; Marschilok, A. C.; Tanzil, K.; Kozarsky, E. S.; Zhu, S.; Takeuchi, K. J. Electrochemical Reduction of Silver Vanadium Phosphorus Oxide, $Ag_2VO_2PO_4$: The Formation of Electrically Conductive Metallic Silver Nanoparticles. *Chem. Mater.* **2009**, *21*, 4934−4939.
(34) Bock, D. C.; Takeuchi, K. J.; Marschilok, A. C.; Takeuchi, E. S. Structural and Silver/Vanadium Ratio Effects on Silver Vanadium Phosphorous Oxide Solution Formation Kinetics: Impact on Battery Electrochemistry. *Phys. Chem. Chem. Phys.* **2015**, *17*, 2034−2042.
(35) Bock, D. C.; Marschilok, A. C.; Takeuchi, K. J.; Takeuchi, E. S. A Kinetics and Equillibrium Study of Vanadium Dissolution from Vanadium Oxides and Phosphates in Battery Electrolytes: Possible Impacts on ICD Battery Performance. *J. Power Sources* **2013**, *201*, 219−225.
(36) Bock, D. C.; Takeuchi, K. J.; Marschilok, A. C.; Takeuchi, E. S. Silver Vanadium Oxide and Silver Vanadium Phosphorous Oxide Dissolution Kinetics: A Mechanistic Study with Possible Impact on Future ICD Battery Lifetimes. *Dalton Trans.* **2013**, *42*, 13981−13989.
(37) Ellis, B. L.; Lee, K. T.; Nazar, L. F. Positive Electrode Materials for Li-Ion and Li Batteries. *Chem. Mater.* **2010**, *22*, 691−714.
(38) Kim, D.-H.; Kim, J. Synthesis of $LiFePO_4$ Nanoparticles in Polyol Medium and Their Electrochemical Properties. *Electrochem. Solid-State Lett.* **2006**, *9*, A439−A442.

DOI: 10.1021/am509066n
ACS Appl. Mater. Interfaces 2015, 7, 5429−5437

(39) Iltchev, N.; Chen, Y.; Okada, S.; Yamaki, J.-i. $LiFePO_4$ Storage at Room and Elevated Temperatures. *J. Power Sources* **2003**, *119−121*, 749−754.
(40) Koltypin, M.; Aurbach, D.; Nazar, L.; Ellis, B. On the Stability of $LiFePO_4$ Olivine Cathodes under Various Conditions (Electrolyte Solutions, Temperatures). *Electrochem. Solid-State Lett.* **2007**, *10*, A40−A44.
(41) Kang, H. Y.; Wang, S. L.; Tsai, P. P.; Lii, K. H. Hydrothermal Synthesis, Crystal Structure and Ionic Conductivity of Silver Vanadium Oxide Phosphate, $Ag_2VO_2PO_4$: A New Layered Phosphate of Vanadium(V). *J. Chem. Soc., Dalton Trans. (1972−1999)* **1993**, 1525−1528.
(42) Leising, R. A.; Takeuchi, E. S. Solid-State Cathode Materials for Lithium Batteries: Effect of Synthesis Temperature on the Physical and Electrochemical Properties of Silver Vanadium Oxide. *Chem. Mater.* **1993**, *5*, 738−742.
(43) Crespi, A.; Schmidt, C.; Norton, J.; Chen, K.; Skarstad, P. Modeling and Characterization of the Resistance of Lithium/SVO Batteries for Implantable Cardioverter Defibrillators. *J. Electrochem. Soc.* **2001**, *148*, A30−A37.
(44) Crespi, A. M.; Skarstad, P. M. Rebalancing of Lithium/Silver Vanadium Oxide (Li/SVO) Cells for Cardiac Defibrillators. U.S. Patent 5458997 A, October 17, 1995.
(45) Crespi, A. M. Silver Vanadium Oxide Cathode Material. European Patent EP 0478303 A2, April 1, 1992.
(46) Crespi, A. M.; Somdahl, S. K.; Schmidt, C. L.; Skarstad, P. M. Evolution of Power Sources for Implantable Cardioverter Defibrillators. *J. Power Sources* **2001**, *96*, 33−38.
(47) Gomadam, P. M.; Merritt, D. R.; Scott, E. R.; Schmidt, C. L.; Skarstad, P. M.; Weidner, J. W. Modeling Li/CF_x-SVO Hybrid-Cathode Batteries. *J. Electrochem. Soc.* **2007**, *154*, A1058−A1064.
(48) Ablett, J. M.; Kao, C. C.; Reeder, R. J.; Tang, Y.; Lanzirotti, A. X27A—A New Hard X-ray Micro-Spectroscopy Facility at the National Synchrotron Light Source. *Nucl. Instrum. Methods Phys. Res., Sect. A* **2006**, *562*, 487−494.
(49) Ravel, B.; Newville, M. Athena, Artemis, Hephaestus: Data Analysis for X-ray Absorption Spectroscopy Using IFEFFIT. *J. Synchrotron Radiat.* **2005**, *12*, 537−541.
(50) Kang, H. Y.; Wang, S. L.; Tsai, P. P.; Lii, K. H. Hydrothermal Synthesis, Crystal Structure and Ionic Conductivity of Silver Vanadium Oxide Phosphate, $Ag_2VO_2PO_4$: A New Layered Phosphate of Vanadium(V). *J. Chem. Soc., Dalton Trans.* **1993**, 1525−1528.
(51) Onoda, M.; Kanbe, K. Crystal Structure and Electronic Properties of the $Ag_2V_4O_{11}$ Insertion Electrode. *J. Phys.: Condens. Matter* **2001**, *13*, 6675−6685.
(52) Kirshenbaum, K. C.; Bock, D. C.; Zhong, Z.; Marschilok, A. C.; Takeuchi, K. J.; Takeuchi, E. S. In Situ Profiling of Lithium/$Ag_2VP_2O_8$ Primary Batteries Using Energy Dispersive X-ray Diffraction. *Phys. Chem. Chem. Phys.* **2014**, *16*, 9138−9147.
(53) Gireaud, L.; Grugeon, S.; Laruelle, S.; Yrieix, B.; Tarascon, J. M. Lithium Metal Stripping/Plating Mechanisms Studies: A Metallurgical Approach. *Electrochem. Commun.* **2006**, *8*, 1639−1649.
(54) Shi, S.; Lu, P.; Liu, Z.; Qi, Y.; Hector, L. G.; Li, H.; Harris, S. J. Direct Calculation of Li-Ion Transport in the Solid Electrolyte Interphase. *J. Am. Chem. Soc.* **2012**, *134*, 15476−15487.
(55) Lu, P.; Li, C.; Schneider, E. W.; Harris, S. J. Chemistry, Impedance, and Morphology Evolution in Solid Electrolyte Interphase Films During Formation in Lithium Ion Batteries. *J. Phys. Chem. C* **2014**, *118*, 896−903.
(56) Crans, D. C. Fifteen Years of Dancing with Vanadium. *Pure Appl. Chem.* **2005**, *77*, 1497−1527.
(57) Wanty, R. B.; Goldhaber, M. B. Thermodynamics and Kinetics of Reactions Involving Vanadium in Natural Systems: Accumulation of Vanadium in Sedimentary Rocks. *Geochim. Cosmochim. Acta* **1992**, *56*, 1471−1483.

DOI: 10.1021/am509066n
ACS Appl. Mater. Interfaces 2015, 7, 5429−5437